Supplementary Information

Computer Simulations of Fibronectin Adsorption on Hydroxyapatite Surfaces

Chenyi Liao, [a] Yun Xie[b] and Jian Zhou*[a]

[a] School of Chemistry and Chemical Engineering, Guangdong Provincial Key Lab for Green Chemical Product Technology, South China University of Technology, Guangzhou, 510640, P. R. China

[b] School of Chemistry and Chemical Engineering, Guangdong Pharmaceutical University, Guangzhou, 510006, P. R. China

* Corresponding author. Telephone: +86-20-87114069; Fax: +86-20-87114069;

E-mail address: jianzhou@scut.edu.cn (J. Zhou)

Contents

S1. Crystal geometry and HAP force field parameterization.

The original crystal structure of HAP ($P6_3$/m) was extracted from the American Mineralogist Crystal Structure Database[1]. The defective HAP (001) surface is cut with half the Ca(1) ions presented in the upper and lower interface[2] (see Fig. S1a) by Material Studio 4.4 (Accelrys, Inc.).
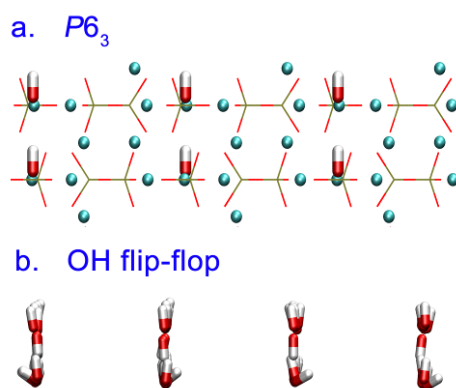

Fig. S1 (a) $P6_3$ structure of hexagonal HAP; (b) the protonic disorder within the OH column during MD process (OH flip-flop).

The all-atom force field parameters for HAP were derived from Hauptmann's model,[3] which is fitted into Lennard-Jones potential.[4] Partial charges[3] and VDW parameters[4] for different HAP atom types are list in Table S1. The LJ parameters for HAP force field were used in other

2

studies[4, 5] and were also evaluated before used in present paper. The bulk crystal lattice parameters of HAP (in $P6_3$ space group) are computed in MD simulations. The system contains 4×4×5 HAP crystal units in a periodic box. Cutoff distance of 1.3 nm is adopted for short-range non-bonded forces. Bonds were constrained by the LINCS algorithm.[6] Particle Mesh Ewald (PME),[7] modified Berendsen thermostat (V-rescale)[8] and Parrinello-Rahman[9] methods were used. The simulation ran 3 ns in NPT ensemble. At 310 K, the LJ parameters provide an average deviation of 0.7% (see Table S2).

Table S1. Partial charges and VDW parameters for different HAP atom types used in MD simulations.

Atom	Charge (e)	ε (kJ·mol^{-1})	σ (nm)
Ca	+2.0	0.49635	0.29413
P	+2.6	4.07547	0.34857
O(P)	-1.4	1.05441	0.30325
O(H)	-1.6	0.48965	0.30929
H	+0.6	0.00004	0.14042

Table S2. Simulated and experimental[1] HAP unit cell parameters at 310 K.

	a (nm)	b (nm)	c (nm)	α	β	γ
Simu.	0.9358	0.9358	0.6835	90	90	120
Exp.	0.9423	0.9423	0.6883	90	90	120

There are two different HAP phases, hexagonal and monoclinic, found in nature. Only the former is of great relevance in biological binding.[10] The hexagonal HAP with $P6_3$/m space group is often reduced to $P6_3$ space group which has all OH groups pointing to the same direction in each column (see Fig. S1a). From a thermodynamic point, the monoclinic phase ($P2_1$/b space group) with anti-parallel OH groups in alternate neighboring columns is more stable than $P6_3$ form.[10] However, in studies of HAP slabs, $P6_3$ form is found to keep the phosphate groups alignment better than monoclinic form as the phosphate groups between anti-parallel OH groups tend to tilt slightly (see Fig. S2). Also, the ferroelectric OH$^-$ alignment in $P6_3$ form was found to show no harm to the stability of the HA (001) surface at a nanometric scale.[11] In present study, the $P6_3$ phase is adopted because: (1) the $P6_3$ space group keeps the feature of hexagonal HAP furthest; (2) the MD process allows the OH flip-flop, i.e., it is also an equilibrium process for HAP slab (see Fig. S1b); (3) we care more about the influence of surface property on protein adsorption instead of the effect of bulk property. The defective surface with Ca(1) vacancies (see Fig. S1a) was investigated here. The total electrostatic effect of this surface is more like a weakly

positively charged surface according to the outermost surface charged density and ions distribution (see Fig. S3 (a, b)).
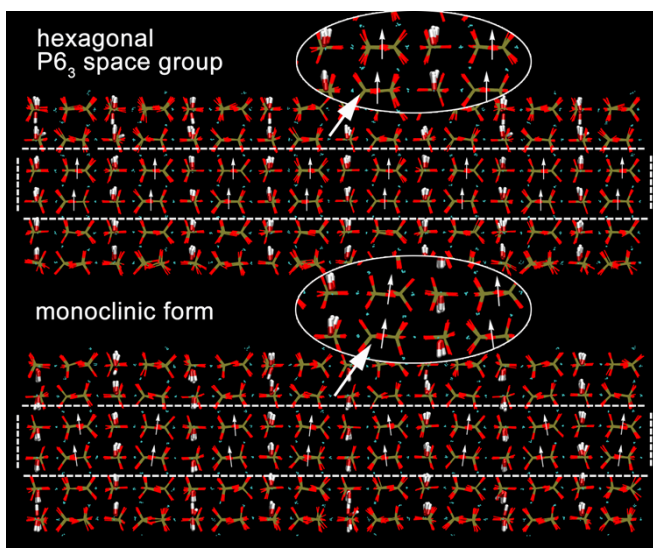

Fig. S2 HAP with hexagonal $P6_3$ form and monoclinic form during MD simulations.
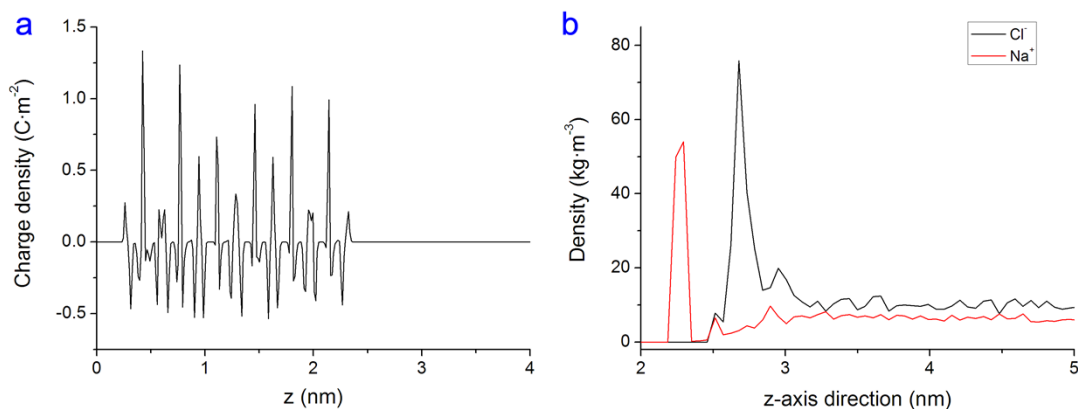

Fig. S3 Charged density profile of studied HAP slab (a) and density profiles of Na^+ and Cl^- ions along z-axis direction (b). Na^+ ions tend to fill the Ca(1) vacancies on surface (around z = 2.29 nm), while Cl^- ions tend to gather at 0.4 nm from the surface (at about z = 2.68 nm). The ions densities decay with increasing distance from the surface, and approach bulk solution conditions.

S2. Overlap of energy distribution and the repeatability of PTMC method

As shown in Fig. S4, the overlap of energy distribution with temperature distribution of (310, 500, 800, 1500, 2500 K) in FN-III10 system (SCD = 0.008 $C \cdot m^{-2}$, IS = 0.02 M) is sufficient to

allow swaps. To test the repeatability of PTMC approach, simulations with five different initial configurations were carried out with the same parameters. As shown in Fig. S5, the orientation distributions of FN-III10 system (SCD = -0.005 C·m^{-2}, IS = 0.02 M) with five different initial configurations repeat well.

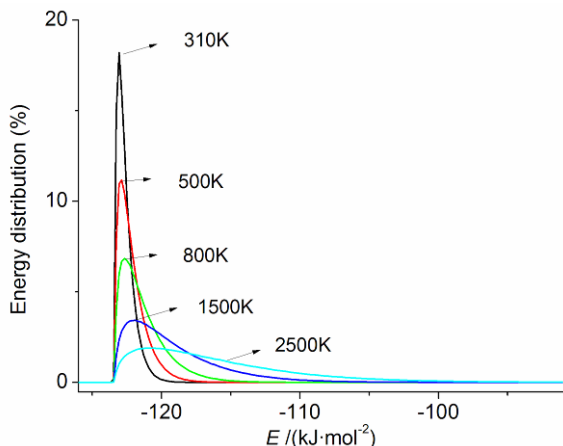

Fig. S4 Energy distribution in FN-III10 system (SCD = 0.008 C·m^{-2}, IS = 0.02 M).

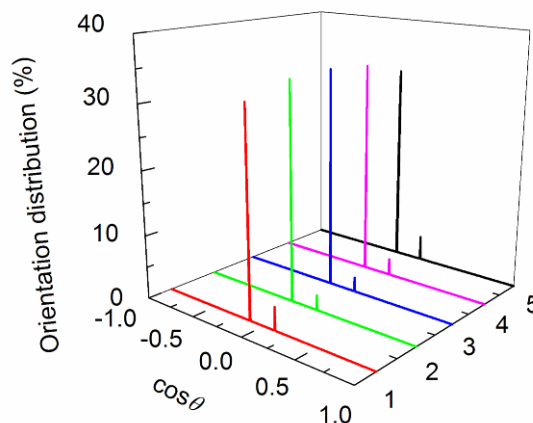Fig. S5 Orientation distributions of FN-III10 system (SCD = -0.005 C·m^{-2}, IS = 0.02 M) with five different initial configurations.

S3. Detailed results for FN-III10-HAP and FN-III7-10-HAP system in PTMC

Energy terms in PTMC. The total potential energy (U_{tot}), VDW potential energy (U_{VDW}), electrostatic potential energy (U_{ele}) and the percentage (P) of major orientations for each protein are listed in Tables S3-4. At some conditions, there exist multiple orientations. The relationship between the probability of a specific configuration and its energy is

$$P_i = \frac{\exp(-U_i/kT)}{\sum_i \exp(-U_i/kT)}, \tag{3}$$

U_i is the adsorption energy of configuration i, k is the Boltzmann constant, and T is the temperature. 1 kT corresponds to 2.58 kJ·mol^{-1} at 310 K. Any configuration whose adsorption energy is 17.1 kJ·mol^{-1} higher than the lowest one will be discarded, since the probability of appearance for this orientation will be less than 0.1%.[12]

FN-III10-HAP system. The preferred "side-on" orientation adjusting slightly with $\cos\theta$ from 0.467 to 0.36 is shown in Fig. S6. The energy terms for FN-III10 orientations are listed in Table S3.
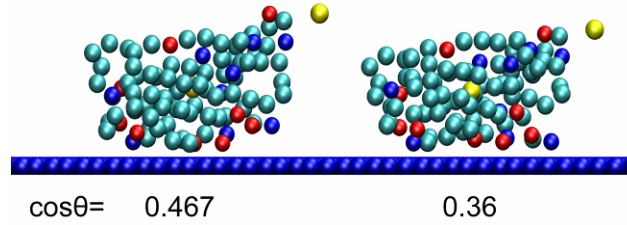

$\cos\theta=$ 0.467   0.36

Fig. S6 Orientation ($\cos\theta$) of FN-III10 adjusting slightly from 0.467 to 0.36 in coarse-grained model. The yellow beads represent the dipole direction. The configuration difference is not significant. Thus, we classify them as one kind.

Table S3 Energies and orientations of FN-III10 adsorbed on different charged surfaces

SCD (C·m⁻²)	IS (M)	U_{tot} (kJ·mol⁻¹)	U_{vdw} (kJ·mol⁻¹)	U_{ele} (kJ·mol⁻¹)	Orientation ($\cos\theta$)	Fig.	P (%)
-0.025	0.005	-291.2	-49.9	-241.3	"head-on" (-0.781)	3a	100
	0.02	-172.3	-104.0	-68.3	"lying-1" (0.109)	3c	100
	0.154	-153.9	-104.1	-49.8	"lying-1" (0.109)	3c	93.86
		-142.7	-115.6	-27.1	"lying-2" (-0.137)	3b	6.14
	0.3	-127.6	-115.2	-12.3	"lying-2" (-0.137)	3b	69.09
		-125.2	-104.0	-21.2	"lying-1" (0.109)	3c	30.91
-0.005	0.005	-132.3	-111.5	-20.8	"lying-2" (-0.137)	3b	71.65
		-130.1	-103.7	-26.4	"lying-1" (0.109)	3c	28.35
	0.02	-120.5	-110.4	-10.2	"lying-2" (-0.137)	3b	80.92
		-116.7	-103.6	-13.1	"lying-1" (0.109)	3c	19.08
	0.154	-111.2	-108.2	-3.0	"lying-2" (-0.137)	3b	94.02
		-108.1	-103.6	-4.5	"lying-1" (0.109)	3c	5.98
	0.3	-110.0	-108.3	-1.7	"lying-2" (-0.137)	3b	93.52
		-106.6	-103.6	-3.0	"lying-1" (0.109)	3c	6.48
0.025	0.005	-269.3	-88.2	-181.1	"side-on" (0.436)	3d	100
	0.02	-189.3	-88.9	-100.4	"side-on" (0.436)	3d	100
	0.154	-170.4	-95.0	-75.4	"side-on" (0.467)	3d	100
	0.3	-149.3	-95.5	-53.8	"side-on" (0.467)	3d	100
0.008	0.005	-152.8	-95.9	-56.9	"side-on" (0.467)	3d	100
	0.02	-123.0	-95.8	-27.1	"side-on" (0.467)	3d	72.32
		-120.1	-108.7	-11.4	"side-on" (0.36)	3d	27.68

0.154		-113.1	-110.6	-2.5	"side-on" (0.36)	3d	92.08
		-106.7	-111.3	4.6	"lying-2" (-0.137)	3b	7.92
0.3		-112.2	-114.9	2.7	"lying-2" (-0.137)	3b	70.72
		-110.2	-109.0	-1.2	"side-on" (0.36)	3d	29.29

FN-III7-HAP system. The energy terms for FN-III7-10 orientations are listed in Table S4.

Table S4 Energies and orientations of FN-III7-10 adsorbed on different charged surfaces

| SCD (C·m^{-2})	IS (M)	U_{tot} (kJ·mol^{-1})	U_{vdw} (kJ·mol^{-1})	U_{ele} (kJ·mol^{-1})	Orientation (cosθ)	Fig.	P (%)
-0.025	0.005	-228.7	-104.1	-124.6	"end-on" (-0.701)	4a	100
	0.02	-161.1	-104.5	-56.6	"end-on" (-0.701)	4a	100
	0.154	-126.5	-104.8	-21.7	"end-on" (-0.701)	4a	100
	0.3	-119.2	-104.9	-14.3	"end-on" (-0.701)	4a	100
-0.005	0.005	-120.1	-104.7	-15.5	"end-on" (-0.701)	4a	100
	0.02	-114.6	-104.6	-10.0	"end-on" (-0.701)	4a	100
	0.154	-141.6	-157.0	15.4	"lying" (0.11)	4b	95.21
		-130.6	-140.3	9.7	"side-on" (0.289)	4c	4.79
	0.3	-148.3	-157.1	8.8	"lying" (0.11)	4b	97.06
		-135.1	-140.3	5.1	"side-on" (0.289)	4c	2.94
0.025	0.005	-1013.3	-153.0	-860.3	"lying" (0.11)	4b	100
	0.02	-570.5	-152.8	-417.7	"lying" (0.11)	4b	100
	0.154	-245.6	-152.6	-92.9	"lying" (0.11)	4b	100
	0.3	-213.5	-152.2	-61.3	"lying" (0.11)	4b	100
0.008	0.005	-416.0	-153.1	-263.0	"lying" (0.11)	4b	100
	0.02	-266.8	-152.8	-114.0	"lying" (0.11)	4b	100
	0.154	-178.8	-152.5	-26.3	"lying" (0.11)	4b	100
	0.3	-167.1	-152.5	-14.6	"lying" (0.11)	4b	100

S4. Improper initial orientation of FN-III10 on HAP surface
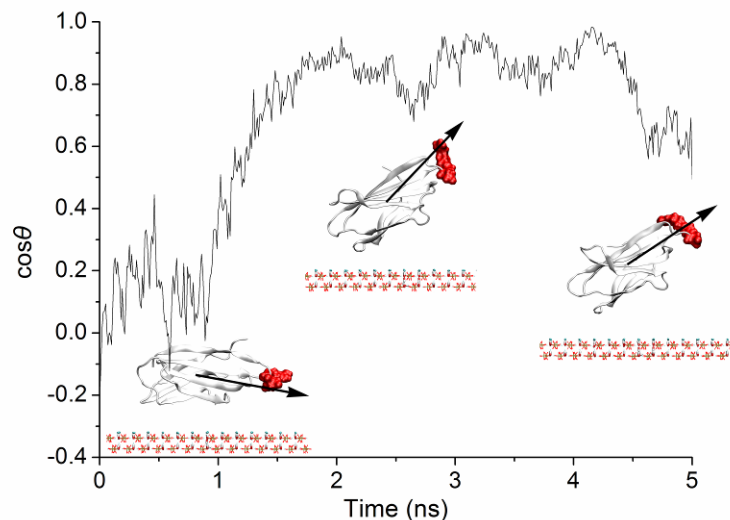
Fig. S7 Time evolution of FN-III10 orientation (cosθ) with improper initial orientation on HAP surface in 5 ns MD. The RGD residues are in red. Dipole direction of protein is presented as a black arrow.

In 5 ns MD, FN-III10 with improper initial orientation rotates significantly with RGD sequence from downward to upward.

S5. Water effect of FN-III10 on HAP surface.

The energy and distance values suggest that FN-III10 has adsorbed on the HAP surface but the Coulombic interactions between them are not so favorable. The less strong interactions make us consider about its stability of adsorption on HAP surface.[13] Thus, we extend the simulation time to 100 ns after FN-III10 steps into the post-adsorption stage at around 20 ns. We found that the orientation and structure of FN-III10 are stable, the protein-HAP distance keeps low and even lower regardless of the less strong protein-HAP interactions. In an aqueous environment, the adsorption on a charged and hydrophilic surface like HAP usually involve the competitive adsorption between protein and water.[14] In order to find out the role that water molecules play during the adsorption in our simulation system, we check the water layers between FN-III10 and HAP within 0.6 nm (Fig. S8a) and distribution of water density along z-axis direction in the initial 8 ns and last 50 ns in comparison with that in water-HAP system as shown in Fig. S8b. Unlike the highly ordered water layer on TiO_2 surface,[15] the water layer tends to be more freely

8

adsorbed on HAP surface. There is about 0.35 nm water layers between the protein and HAP. The water density at 0.37 nm away (z = 2.46 nm) from HAP surface in water-HAP system is higher than it in protein-HAP system (see Fig. S8b). In protein-HAP system, water density at 0.47 nm away (z = 2.56 nm) from HAP surface in the last 50 ns is much lower than it in the initial 8 ns, demonstrating that FN-III10 adsorbs on the HAP surface and local water molecules are expelled. The water molecules between FN-III10 and HAP might weaken the Coulombic repulsion.
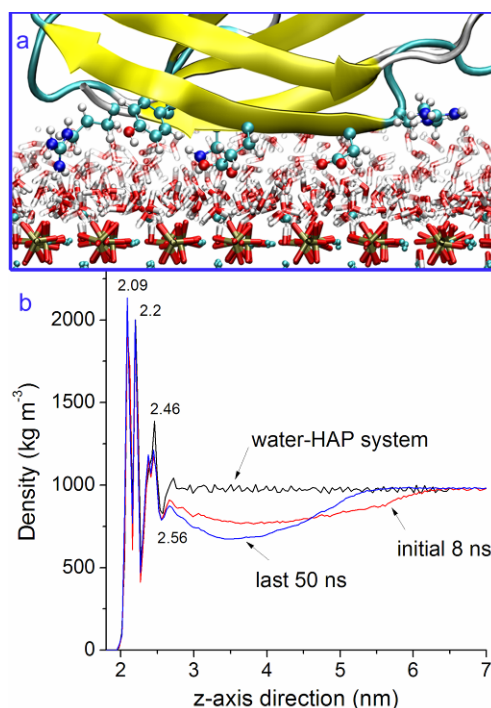

Fig. S8 (a) water layers between FN-III10 and HAP within 0.6 nm at 100 ns. (b) Distribution of water density along z-axis direction in FN-III10-HAP system in initial 8 ns and last 50 ns in comparison with it in water-HAP system. The outermost Ca(1) locates at around z = 2.08 nm.

S6. Surface electrostatic effect of FN-III10 on HAP surface.

What factor causes the Coulombic repulsion between FN-III10 and HAP? We ascribe the total repulsion effect to the mismatching of the acidic, basic and amide residues on the alternative positively and negatively charged regions of HAP surface. After FN-III10 adsorbs stably on HAP surface, we found that it keeps making slight translation on HAP surface during the adsorption. Regardless of water effect, the electric potential difference generated by the

alternative positively and negatively charged regions on HAP surface in horizontal direction may drive the acidic, basic and amide residues nearby to move horizontally instead of vertically (see Fig. S9). This may explain why repulsion effect between FN-III10 and HAP does not cause FN-III10 to leave away from HAP surface; instead the residues near surface keep translating around.
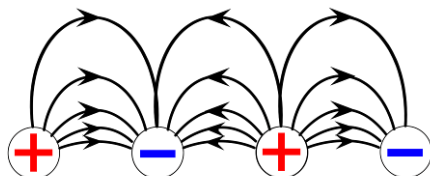

Fig. S9 Field of positive and negative charges on HAP surface.
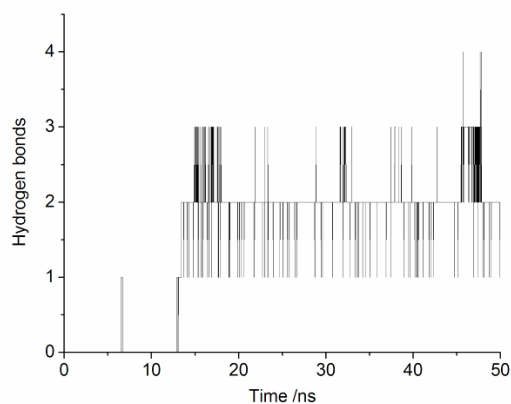
S7. Hydrogen bonds in FN-III7-10 system

Fig. S10 Hydrogen bonds formed between FN-III7-10 and HAP surface.
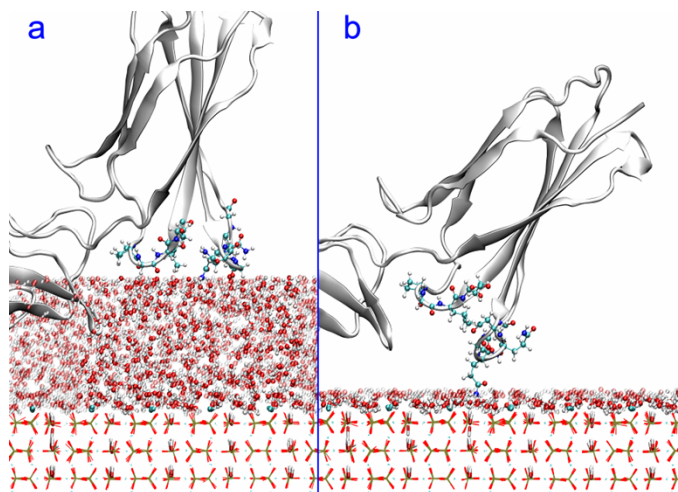
S8. Water layer in FN-III7-10 system

Fig. S11 Water layer between module III7 and HAP surface. (a) snapshot at 40.4 ns; (b) snapshot at 49.7 ns.

References

1. R. M. Wilson, J. C. Elliott and S. E. P. Dowker, *Am. Mineral.*, 1999, **84**, 1406-1414.
2. D. Zahn and O. Hochrein, *Phys. Chem. Chem. Phys.*, 2003, **5**, 4004-4007.
3. S. Hauptmann, H. Dufner, J. Brickmann, S. M. Kast and R. S. Berry, *Phys. Chem. Chem. Phys.*, 2003, **5**, 635-639.
4. R. Bhowmik, K. S. Katti and D. Katti, *Polymer*, 2007, **48**, 664-674.
5. A. K. Nair, A. Gautieri, S.-W. Chang and M. J. Buehler, *Nat Commun*, 2013, **4**, 1724.
6. B. Hess, H. Bekker, H. J. C. Berendsen and J. G. E. M. Fraaije, *J. Comput. Chem.*, 1997, **18**, 1463-1472.
7. T. Darden, D. York and L. Pedersen, *J. Chem. Phys.*, 1993, **98**, 10089.
8. G. Bussi, D. Donadio and M. Parrinello, *J. Chem. Phys.*, 2007, **126**, 014101.
9. M. Parrinello and A. Rahman, *J. Appl. Phys.*, 1981, **52**, 7182-7190.
10. M. Corno, A. Rimola, V. Bolis and P. Ugliengo, *Phys. Chem. Chem. Phys.*, 2010, **12**, 6309-6329.
11. F. Chiatti, M. Corno and P. Ugliengo, *J. Phys. Chem. C*, 2012, **116**, 6108-6114.
12. J. Zhou, S. Chen and S. Jiang, *Langmuir.*, 2003, **19**, 3472-3478.
13. T. Wei, M. A. Carignano and I. Szleifer, *Langmuir.*, 2011, **27**, 12074-12081.
14. A. Rimola, M. Corno, C. M. Zicovich-Wilson and P. Ugliengo, *Phys. Chem. Chem. Phys.*, 2009, **11**, 9005-9007.
15. T. Utesch, G. Daminelli and M. A. Mroginski, *Langmuir.*, 2011, **27**, 13144-13153.